Mean Field Modeling of Grain Growth and Zener Pinning

Kaisheng Wu[1] · Johan Jeppsson[2] · Paul Mason[1]

Abstract A mean-field model has been developed to simulate curvature-driven grain growth by exploring the evolution of grain size distribution under arbitrary thermal histories. The model was integrated into precipitation module TC-PRISMA, so that the pinning effect of the concurrently precipitated particles on the growing grains can be considered by a modified, location-specific Zener model. The developed model was validated against analytical calculations, and then applied to real alloy systems, fed with assessed grain boundary energy and mobility data. Its capabilities, limitations, and directions to improvements have been discussed.

Keywords grain growth · kinetics · microstructure · modeling · Zener pinning

✉ Kaisheng Wu
  kaisheng@thermocalc.com

1 Thermo-Calc Software Inc., McMurray, PA

2 Thermo-Calc Software AB, Solna, Sweden

1 Introduction

The progress of incorporating computational techniques into materials research and development has been gaining remarkable momentum in recent years, not only by increasing demand from traditional metallurgical industries and emerging new areas such as additive manufacturing and high entropy alloys, but also by strategic projects such as Integrated Computational Materials Engineering (ICME) and Materials Genome Initiative (MGI). There have been countless efforts to seek synergy of models across different research areas and disciplines. Prof. John Morral has been regarded as a model scientist in solid state phase transformations who tirelessly broke research barriers throughout his career. He and Purdy developed a coarsening model for precipitation kinetics[1] that has been widely used in various programs such as TC-PRISMA[2] whose development the authors have been heavily involved in. Particularly, Prof. Morral was an inspiring mentor to one of the current authors (KW) and also encouraged and guided him to employ phase field method to the investigation of interdiffusion microstructures.[3]

The first purpose of the current work attempted to extend the functionality of the precipitation program TC-PRISMA to account for more microstructure information. In solid state, grain structure plays such a critical role that, to many researchers, it is the synonym of microstructure. The attempt started with the investigation of normal grain growth, and subsequently its efficient modeling that is compatible with the existing precipitation tool. Therefore, a mean field approach has been favored and thus implemented. The "normal", or "continuous", grain growth is defined as the average size increase of space-filling grains with somewhat uniform size distributions, that is driven by the curvatures, or the surface tensions (boundary energies)

of their adjacent boundaries.[4,5] In metallurgical applications, these grains often refer to the polycrystals of the matrix phase, which most likely contain other dispersed second-phase particles. The driving force leads the curved boundary to migrate toward its center of curvature. The velocity, assuming a linear proportionality, is described as $-M\gamma\kappa$,[6] where M is the proportion coefficient, herein after called grain boundary mobility. γ is the grain boundary energy while κ is the curvature. The rate of change of the volume of each individual grain is thus $-M\gamma$ times the integral of the mean curvature of all surrounding boundaries.[7]

While mathematical integration of the mean curvature over all the boundaries is a daunting task, von Neumann found a surprisingly simple yet elegant expression for a curvature-driven domain growth in two-dimensional space, regardless of the shape of the domain[8]

$$\frac{dA}{dt} = -2\pi M\gamma \left(1 - \frac{1}{6}n\right) \tag{Eq 1}$$

where $\frac{dA}{dt}$ is the rate change of the domain area, and n is the number of triple junctions around the domain. If the domain is assumed to be a circle with radius R so that $dA = 2\pi R dR$, Eq 1 can be re-arranged as

$$\frac{dR}{dt} = M\gamma \left(\frac{1}{\frac{6}{n}R} - \frac{1}{R}\right) \tag{Eq 2}$$

which insightfully implies that the growth rate is related to its curvature (proportional to $1/R$) in comparison to the mean curvature of the whole system (a regular, uniform hexagonal structure with $n = 6$). The same can also been shown in three-dimensional space, while MacPherson and Srolovitz derived three-dimensional rate change of domain volume as[9]

$$\frac{dV}{dt} = -2\pi M\gamma \left[L(\boldsymbol{D}) - \frac{1}{6}\sum_{i=1}^{n} e_i(\boldsymbol{D})\right] \tag{Eq 3}$$

where $L(\boldsymbol{D})$ measures the linear size of domain $\boldsymbol{D}$ and e_i the length of triple line (edge) i summed over all n triple lines of $\boldsymbol{D}$. Replacing volume change with $dV = 4\pi R^2 dR$, a similar formulation to Eq 2 can be obtained. These theories justified the validity of the mean field approach proposed by Hillert,[4] an analogy to the coarsening theory in dispersed second-phase precipitation.[10,11] The mean field approach enables the description of grain structures using grain size distribution (GSD) instead of average grain size, so that size dependent properties like grain boundary mobilities and misorientations can be investigated in the future.

The second purpose of the current work is to study simultaneous grain growth and precipitation processes. The existence of second phase particles, and their interactions with the migrating grain boundaries, are of wide industrial interest in grain size control practice to achieve desired mechanical properties. Abundant experimental information indicates that grain growth can be drastically reduced, or even completely stopped, in systems with appreciable second-phase particles, indicating that the migration of grain boundary can be effectively dragged when passing through dispersed particles. The first theoretical analysis of the particle inhibition effect came from Zener (quoted by Smith[12]). He suggested that a particle could exert a pinning force, described as a line tension opposite to the migration direction, so that the normal grain growth would be completely inhibited when the grain size reached a critical maximum grain size R_z. In current paper, it is termed "Zener radius" to avoid confusion with other grain size nomenclature. In a general form, it can be expressed as[13]

$$R_z = K \frac{r}{f^m} \tag{Eq 4}$$

where r is the radius of the pinning particles and f the volume fraction of the particles. K is a dimensionless constant and m an exponential index for f. The original Zener pinning theory assumed a maximum pinning force that had $K = 4/3$ and $m = 1$, which has been found to be inconsistent with the experimental information and many modifications have been proposed since then, and a thorough review has been conducted by Manohar et al.[13] When applying to practical cases, many limitations of the Zener theory should be realized. First, while Zener radius refers to the maximum critical grain size that completely stops growing, most experiments ignored the grain size distribution, so that average grain size was used as Zener radius and fitted parameters based on this assumption. Secondly, all the original and modified models adjusted the parameters K and m by relating final grain sizes to precipitate particle size and volume fractions, ignoring the whole precipitation process. Another purpose of the current work is thus to investigate the validity and limitation of the pinning models when grain size distribution is explicitly considered, subjected to the overall precipitation process involving particle nucleation, growth, and coarsening.

2 Model Development

2.1 Normal Grain Growth

The normal grain growth model simulates the temporal evolution of grain size distribution (GSD), analogous to the precipitation simulation implemented in TC-PRISMA using Kampmann and Wagner's numerical algorithm.[14] Therefore, the grain system has been represented by a GSD

868

J. Phase Equilib. Diffus. (2022) 43:866–875

function, $g(R_i, t)$, which describes the number of grains with radius R_i at time t. The grains are assumed of spherical morphology. Following the mean field approach by Hillert[4] in the spirit of von Neumann's theory,[8] the boundary motion of a grain with radius R_i is driven by its curvature. Without pinning force, the boundary migration rate has been described as

$$\frac{dR_i}{dt} = \alpha M \gamma \left(\frac{1}{R_{Cr}} - \frac{1}{R_i} \right) \quad \text{(Eq 5)}$$

where M is grain boundary mobility (m^4/Js) and γ is the grain boundary energy (J/m^2). α is a dimensionless scaling constant, whose value is determined by fitting the numerical results to analytical theory, which will be discussed in the next section. R_{Cr} is the critical grain size. Not necessarily the average grain size, it is determined by volume conservation during grain growth process[15]

$$\frac{dV}{dt} = 4\pi \sum_i \frac{g(R_i, t)R_i^2 dR_i}{dt} = 0 \quad \text{(Eq 6)}$$

where the index i covers all sizes of grains. Substituting Eq 5 into 6 thus enables the calculation of R_{Cr}.

$$R_{Cr} = \frac{\sum_i g(R_i, t)R_i^2}{\sum_i g(R_i, t)R_i} \quad \text{(Eq 7)}$$

In comparison, the average radius is defined as

$$\overline{R} = \left(\frac{\sum_i g(R_i, t)R_i^3}{\sum_i g(R_i, t)} \right)^{1/3} \quad \text{(Eq 8)}$$

2.2 Zener Pinning

When there are n different precipitate phases in the alloy, the pinning force combines contributions from all precipitate particles. As a first approximation, the average particle radius $\overline{r_j}$ of each phase j has been used to calculate its pinning force. The pinning force, P_j (in unit of pressure), from phase j can be evaluated in terms of $R_{z,j}$, the Zener radius defined in Eq 4

$$P_j = \frac{\gamma}{R_{z,j}} = \gamma \cdot z_j \quad \text{(Eq 9)}$$

whereas Zener radius $R_{z,j}$ is more convenient when comparing with grain size and thus more intuitively straightforward, its inverse, z_j, is proportional to the pinning pressure, and thus more fundamentally correlated with the drag force

$$z_j = \frac{1}{R_{z,j}} = \frac{1}{K_j} \cdot \frac{f_j^{m_j}}{\overline{r_j}} \quad \text{(Eq 10)}$$

In current model, different values of K_j and m_j have been selected based on the locations of the precipitate phases, i.e., precipitated homogenously within the matrix phase or along the grain boundaries, in accordance with the fact that grain boundary particles provide larger pinning force.[13,16] The overall pinning effect is the sum of that from all precipitate particles, which also defines the inverse of the overall Zener radius

$$z = \sum_{j=1}^n z_j = \frac{1}{R_z} \quad \text{(Eq 11)}$$

Realizing that the drag force resists the grain boundary motion, no matter whether in the growing (positive velocity) or shrinking (negative velocity) direction, the overall growth rate is expressed as[4]

$$\frac{dR_i}{dt} = \alpha M \gamma \left[\left(\frac{1}{R_{Cr}} - \frac{1}{R} \right) \pm \frac{1}{R_z} \right] \quad \text{(Eq 12)}$$

The negative sign for term $1/R_z$ considers suppressing the growing grains, when

$$\left(\frac{1}{R_{Cr}} - \frac{1}{R} \right) - \frac{1}{R_z} > 0 \quad \text{(Eq 13)}$$

while positive sign considers the dissolving grains, when

$$\left(\frac{1}{R_{Cr}} - \frac{1}{R} \right) + \frac{1}{R_z} < 0 \quad \text{(Eq 14)}$$

and $\frac{dR_i}{dt} = 0$ when R_i lies between these two limits.

3 Results

3.1 Normal Grain Growth

The simulations of normal grain growth only considered a single phase, in a polycrystal system. Two different initial GSDs, one of log-normal distribution with standard deviation $\sigma = 0.2$ and the other of Hillert distribution,[4] have been utilized to simulate the normal grain growth. Log-normal distributions with larger standard deviations ($\sigma > 0.2$) have the risk of introducing abnormally large grains, and hence have not been used.

Figure 1(a) shows their initial GSD shapes. We used a plot of normalized number density distribution (number of grains with a specific radius divided by overall number of grains in the system) versus normalized grain radius (grain radius divided by average grain radius) to illustrate GSD. A reasonable grain boundary energy value of $0.5 J/m^2$ was used, while different grain boundary mobility values, ranging from 10^{-16} to $10^{-12} m^4/Js$, have been used to perform the robustness and validation tests.

The results indicate that the model predicts a steady-state parabolic growth law. A typical result has been shown in Fig. 2. For two different initial GSDs, the grain growth behaviors are almost identical in the steady state, with slight deviations at early stages. The steady-state GSDs for both cases, shown in Fig. 1(b), follow a Hillert distribution, in agreement with the analytical result.[4]

It has been observed from all the numerical experiments that the critical radius, R_{Cr} defined in Eq 7, is rarely the same as the average grain radius $\overline{R}$, defined in Eq 8. In most cases, R_{Cr} has a larger value.

Another purpose of these simulations is to determine the value of α in Eq 5 so that the following parabolic equation can be satisfied

$$\overline{R}^2 - \overline{R_0}^2 = \gamma M(t - t_0) \qquad (Eq\ 15)$$

where $\overline{R_0}$ is the average grain radius when steady state begins at time t_0. The numerical results suggested $\alpha \approx 2.3$, close to the theoretical approximation of $\alpha \approx 2$.[4]

3.2 Zener Pinning

The particle pinning models offer a single parameter, Zener radius R_z, as a criterion for the retarding force. Dealing with non-uniform GSD, the current model does not explicitly provide R_z from the output. Therefore, a numerical experiment has been designed for the validation process. For this purpose, the physical properties of the alloy system are not relevant. Without loss of generality, we selected Al-Sc system which is available from Thermo-Calc's free databases ALDEMO and MALDEMO. The alloy had a composition of Al-4.0 at.% Sc with FCC_A1 as matrix phase and AL3SC as precipitate phase. Same as in normal grain growth studies, two initial grain size distributions have been employed, with log-normal distribution

$\sigma = 0.2$ as well as with Hillert distribution.[4] A series of numerical simulations have then been carried out, each varied in average radius and volume fraction of precipitate particles so that different pinning forces, and hence Zener radii, could be generated. The Zener radius R_z of these simulations, calculated using Eq 4, varied from 1 to 0.1 mm. Since both, the theoretical model and the current model, do not consider particle size distribution (PSD) effect on the pinning force, the choice of PSD can be arbitrary. Theoretical models with different parameters K and m in Eq 4 and 10 have been employed, as listed in Table 1. To avoid the change of the pinning force due to particle growth and coarsening, the precipitating particles have been "frozen", which in TC-PRISMA can be achieved by assigning an extremely small value, e.g. 10^{-15}, to the mobility enhancement pre-factor for bulk solute diffusion in matrix phase, and a small interfacial energy, $0.01 J/m^2$, to the precipitate phase. The grain growth was then continued for an extended period, assuming a grain boundary mobility of $10^{-14} m^4/Js$, and grain boundary energy of $0.5 J/m^2$.

Figure 3 shows a typical temporal change of the average grain sizes as the solid line. At the final stage, the growth kinetics deviates from the parabolic curve and reaches a plateau, indicating that the grain growth has been stopped due to the pinning force. It should be noted that the final average radius, calculated using Eq 8, does not match the Zener radius R_z, but is rather significantly smaller. It has also been found that average grain radius is usually smaller than the critical radius R_{Cr} define in Eq 7, as shown by the dotted line in Fig. 3. The assumption in most theoretical analyses that they are the same, thus are not applicable and can cause inaccuracies in quantitative calculations. A detailed analysis of the GSD is thus needed to validate R_z. Figure 4 shows the comparison of the initial (dotted line)
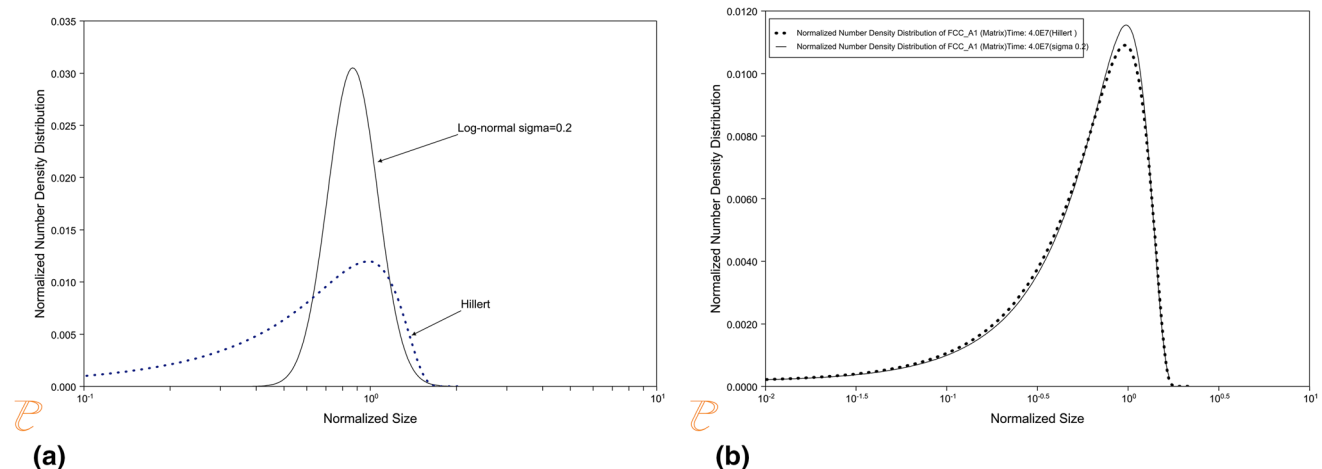

Fig. 1 (a) Initial and (b) steady-state grain size distributions for normal grain growth. The solid line has an initial log-normal distribution, and the dashed line has an initial Hillert distribution
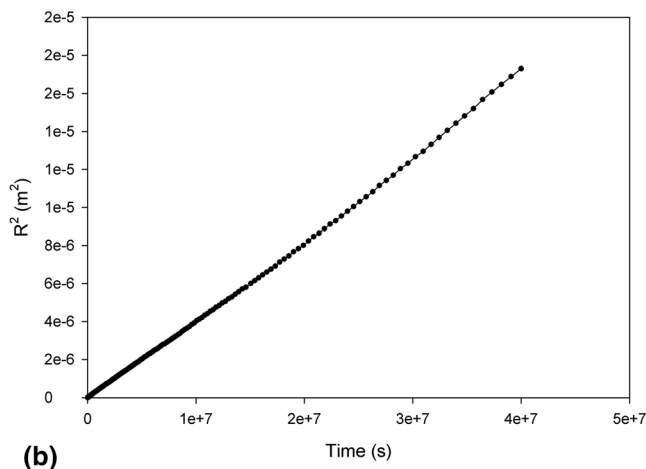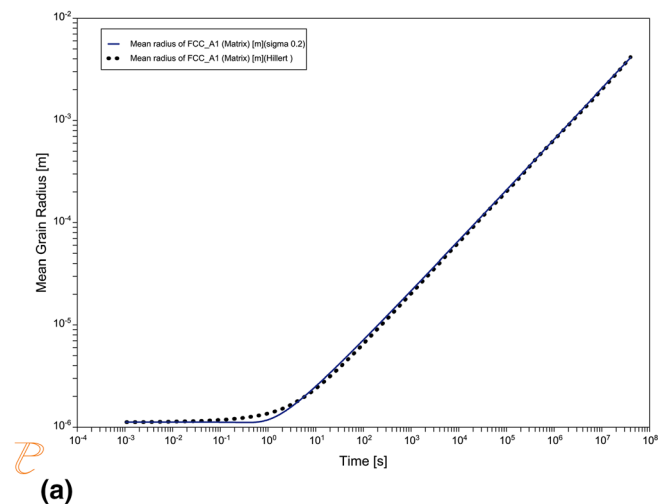
(a)

(b)

Fig. 2 (a) Calculated temporal change of average grain size, with initial GSD of log-normal (solid line) and Hillert (dashed line) distribution (b) Plot of square of average grain size with time.

Simulated with grain boundary mobility $M = 10^{-12} \mathrm{m}^4/\mathrm{Js}$, and grain boundary energy $\gamma = 0.5 J/\mathrm{m}^2$

Table 1 Parameters used in Zener equation for validation purpose

K	m	Refs.
1.333	1.0	Zener[12]
0.222	0.93	Hillert[16]
1.333	0.93	Zener[12] + Hillert[16]
1.7	0.5	Hillert[16]
0.17	1.0	Manohar et al.[13]

and final (solid line) GSD when particle pinning has been enabled. Unlike the Hillert distribution that was shown for

a precipitate-free system, the final GSD presents a triangular, jib sail shape. Comparing with the initial GSD, the shape is significantly narrower. Whereas the higher side shrinks due to the reduction of the growth rate, there is a distinct "cut" on the lower size so that the smallest size can be determined easily. This is because that smaller grains have faster dissolution rate that can escape from the precipitate particles and thus disappear completely. The size of the smallest grain, R_m, is determined by Eq 14, using equal sign instead

$$\left(\frac{1}{R_{\mathrm{Cr}}} - \frac{1}{R_m}\right) + \frac{1}{R_z} = 0 \qquad \text{(Eq 16)}$$

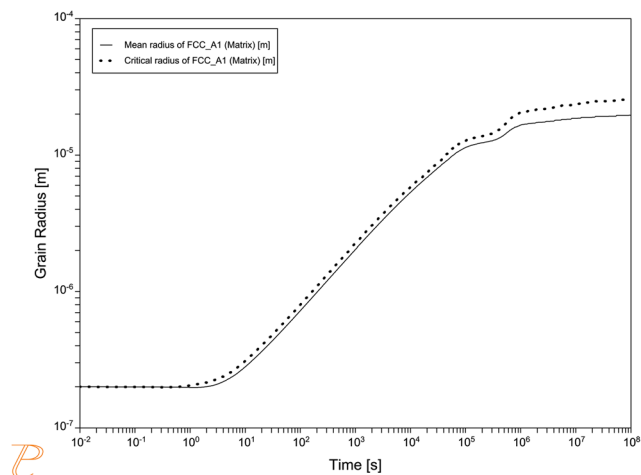Re-arranging Eq 16 we may thus obtain

Fig. 3 The temporal change of average grain size (solid line) and critical radius (dotted line) with Zener pinning. The initial grains have a log-normal distribution with standard deviation $\sigma = 0.2$. The precipitate particles have fixed size of $1.9\mu m$ and volume fraction of 0.08. Zener parameters of $K = 4/3$ [12] and $m = 0.93$ [16] have been used, given a Zener radius $R_z = 26.528\mu m$ according to Eq 4
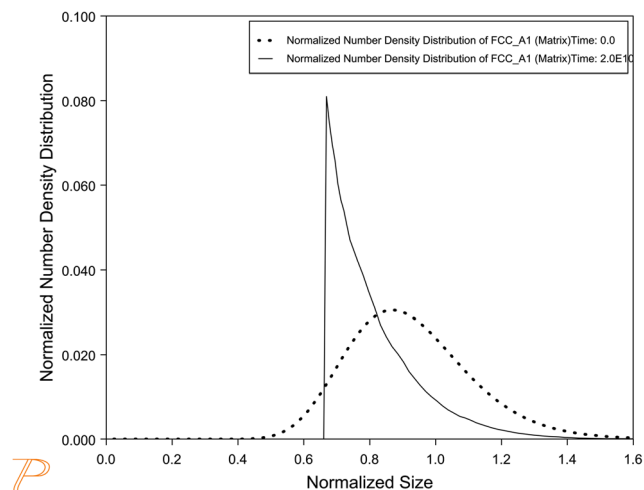

Fig. 4 The initial (dotted line) and final (solid line) grain size distribution, with the same pinning parameters used in Fig. 3

$$R_z = \frac{R_{\mathrm{Cr}}R_m}{R_{\mathrm{Cr}} - R_m} \qquad (Eq\ 17)$$

Therefore, R_z can be calculated from the numerical results of R_{Cr} and R_m. Figure 5 shows the comparison of R_z from theoretical analysis, Eq 4 and from numerical calculations, Eq 17. An excellent agreement has been obtained. Another important observation is that the ratio of R_m to R_{Cr} is around 0.5 to 0.6, less than 0.75 that was assumed in the theoretical analysis by Hellman and Hillert.[17] In their work, the value of 0.75, and further $R_{\mathrm{Cr}} = \overline{R}$, were used to derive Zener parameters K and m for the limiting average grain size $\overline{R}$ in terms of volume fraction and size of the precipitate particles. They admitted that this choice was quite arbitrary and suggested careful experimental comparisons. The current numerical results confirm their concerns. As a result, adjustment of Zener parameters is required to reflect the discrepancy. It is interesting to notice that for $R_m = 0.5R_{\mathrm{Cr}}$, Eq 17 has $R_{\mathrm{Cr}} = R_z$. The simulations with log-normal initial GSD and narrower size range ($\sigma = 0.2$) closely agree with this condition, as shown with empty circles in Fig. 5.

The next numerical experiment employed a commercial steel alloy to study the validity of the Zener model through the simultaneous grain growth and precipitation processes. The composition of the steel alloy is listed in Table 2. The alloy system consists of ferrite (named BCC_A2 in databases) as matrix phase and cementite (CEMENTITE_D011) as precipitate phase. TCFE12 and MOBFE7
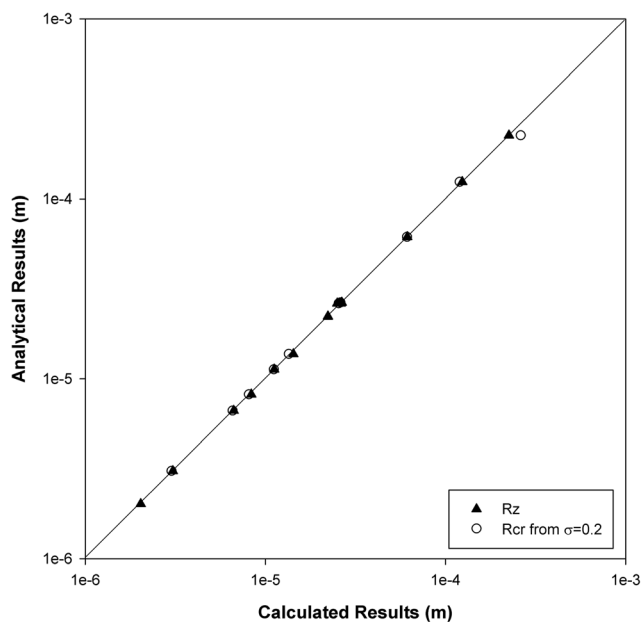

Fig. 5 Calculated Zener radius (filled triangles) against analytical results[16]. The straight line represents a perfect match. The calculated critical grain radii from initial log-normal grain size distribution with $\sigma = 0.2$ are also shown as open circles

databases have been used for precipitation simulation process. To fit the experimental data, a mobility enhancement pre-factor of 0.2 was used, while all other parameters were chosen as default settings in TC-PRISMA. A good agreement in precipitation kinetics for annealing isothermally at 722 °C, with experimental data[17] has been obtained, as shown in Fig. 6. Also shown in the figure is the volume fraction change during the annealing, indicating that the current setting leads to a volume fraction quickly approaching the equilibrium value.

For grain growth simulations, the grain boundary energy was chosen to be a reasonable value of 0.5 J/m² as in previous calculations. The grain boundary mobility has been modeled as an Arrhenius type

$$M = M_0 \exp\left(-\frac{Q}{RT}\right) \qquad (Eq\ 18)$$

where M_0 is the pre-factor (m⁴/Js) and Q is the activation energy (J/mol). There is a large discrepancy, in several orders of magnitude, among experimental data regarding the grain boundary mobility. The experimental grain growth data from Hellman and Hillert[17] indicate that, for this commercial alloy, the grain boundary mobility should be in the magnitude of 10^{-16}m⁴/Js. The closest match was from Malow and Koch,[18] though their data, obtained from nanocrystalline structures which reduce the grain boundary mobility, are thus underestimated for the micro scale grains. Therefore, the activation energy of $242,000$J/mol was adopted from their work, while the grain boundary mobility pre-factor was increased to 4×10^{-3}m⁴/Js, providing a grain boundary mobility of 7.9432×10^{-16}m⁴/Js at 722 °C.

The first attempt used a set of $K = 0.222$ and $m = 0.93$ from Hillert[16] to calculate the pinning force. That gives a Zener radius of about 8 μm according to Eq 4 with final precipitate size and volume fraction data from experiment.[17] The initial GSD was assumed to be a Hillert distribution. Numerical tests indicate that the initial average grain size has a profound effect on the growth behavior. Two of the results are presented in Fig. 7, one with a small initial radius of 0.2 μm (Fig. 7a) and the other with a larger initial radius of 3.2 μm (Fig. 7b). Without pinning force, the grain growth curves (dashed) for both cases follow a parabolic law as expected. When particle pinning has been generated, on the other hand, they display completely different growth paths. The grain growth with a

Table 2 Steel composition (wt.%)[17]

C	S	O	N	Al	Fe
0.2	0.004	0.0004	0.001	0.001	Bal

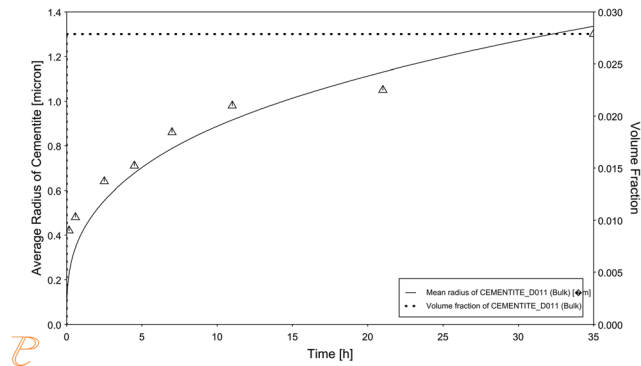872

J. Phase Equilib. Diffus. (2022) 43:866–875

Fig. 6 Calculated average particle radius of cementite (solid line) in comparison with experimental data[17], together with calculated volume fraction change (dashed line)

smaller initial grain size shows discontinuous, stepwise behavior with three distinct plateaus. The first plateau occurs at a very early stage over a very short period, when cementite phase starts to nucleate. Since the size of cementite nuclei is quite small while the volume fraction quickly approaches to the equilibrium volume fraction, the cementite particles exert a larger pinning force, i.e., smaller Zener radius, according to Eq 4. As the initial grain size was small and below the Zener radius, the grains stop growing when reaching the Zener radius. As the cementite particles enter fast growing stage, the pinning effect has been loosened so that the ferrite grains can break and grow sharply. The sharp increase in growth rate is since during the previous plateau, smaller grains have been dissolved leading to a narrower, more uniform GSD shape, and hence a much faster growth rate. The grain growth thus outpaces the precipitate growth, until the grain size reaches the updated Zener radius which then leads to the second plateau. The same process repeats until the third and final

plateau occurs and stabilizes since the precipitate particles coarsen slowly and the grain size reaches the somewhat stable Zener radius. During the multi-step stages, the smaller particles disappear, so that the average grain size increases and is thus closer to the predicted Zener radius.

While the above test with small initial grain size demonstrates possible complicated grain growth phenomena, the second example with an initial grain size of $3.2 \mu m$ seems to be more consistent with the experimental initial grain size.[17] The growth behavior, shown in Fig. 7(b), presents a continuous growth curve, with a growth rate much smaller than that of pinning-free growth and deviation from the parabolic law. The early discontinuous, step stages have been avoided since the initial average grain size is larger than the Zener radius of the precipitate nuclei, and precipitate particles grow faster so that they are unable to withstand the migrating grain to a smaller size. Comparing with the previous case, the loss of the smaller grains is much less, so that the average grain size is significantly smaller than the predicted Zener radius. As a result, the calculated average grain size is much smaller than the experimental data which have been assumed equal to Zener radius and hence were used to fit Zener parameters. Therefore, Zener parameters need to be adjusted to provide a larger Zener radius to match the experimental data. A closer examination of the experimental grain size data appears to imply that the early stage of grain growth follows the parabolic law, corresponding to an un-pinning state. Therefore, the current version of Zener model overly suppresses grain growth when grain size is significantly smaller than Zener radius. By somewhat arbitrarily disabling pinning effect until the average grain size reached $0.7 \mu m$, and setting $K = 0.5$, $m = 0.93$ in Eq 4, the
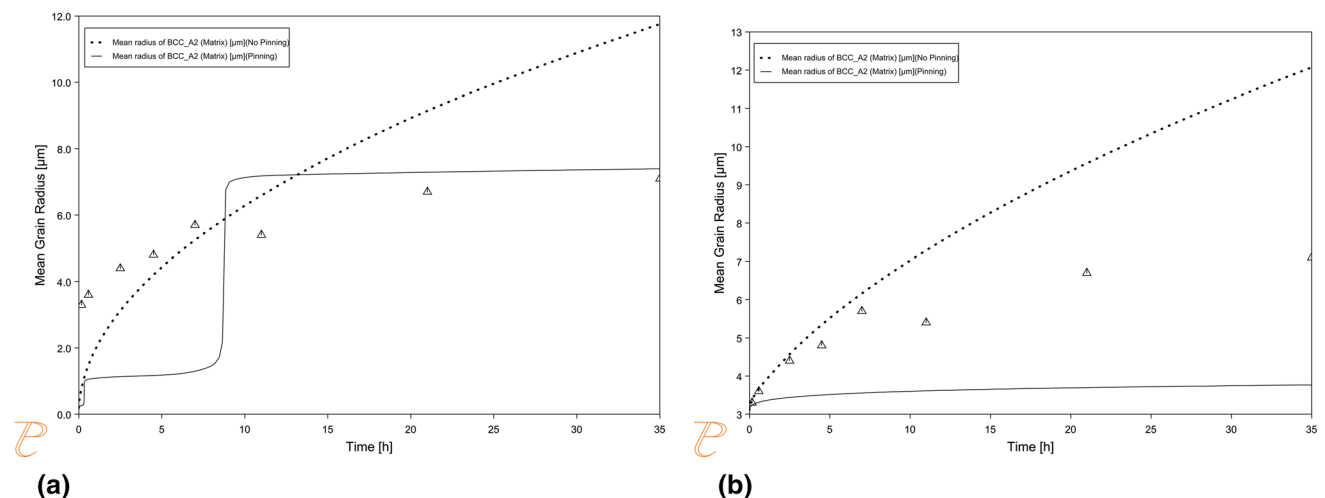

(a)

(b)

Fig. 7 Calculated average grain size and comparison between un-pinned (dashed line) and pinned (solid line) grain growth (a) Initial average grain radius of 0.2 μm (b) Initial average grain radius of 3.2 μm

simulation has been repeated and results are shown in Fig. 8. An excellent agreement has been obtained.

4 Discussions

A general form of the kinetics of normal grain growth can be described as[19]

$$\overline{R}^n - \overline{R_0}^n = kt \qquad \text{(Eq 19)}$$

where n is the grain growth exponent. Current simulations of normal grain growth validate against a theoretical parabolic growth rate ($n = 2$) as expected. Regardless of the initial GSD, either log-normal or Hillert distribution whose largest size is within 1.6 times the average value, a steady-state Hillert distribution is preserved, in agreement with theoretical analysis.[4] Kim et al. argued, based on theoretical derivation, that the log-normal distribution, despite widely recognized in experimental data, is not a steady-state distribution with $n = 2$.[20] Feltham[21] proposed a growth model for a possible steady-state log-normal distribution while maintaining $n = 2$. In terms of the same parameters as defined in Eq 5 his formulation can be expressed as

$$\frac{dR_i}{dt} = \frac{\alpha M \gamma}{R_i} \ln \frac{R_i}{R_{Cr}} \qquad \text{(Eq 20)}$$

However, our preliminary results (although still too immature to be shown in this paper) did not have a log-normal steady-state GSD using this equation. A closer look at this equation reveals that the dissolution rate of the small grains is still significantly larger than the growth rate of the large grains, leaving a tail at the lower end of GSD moving away from a log-normal shape.
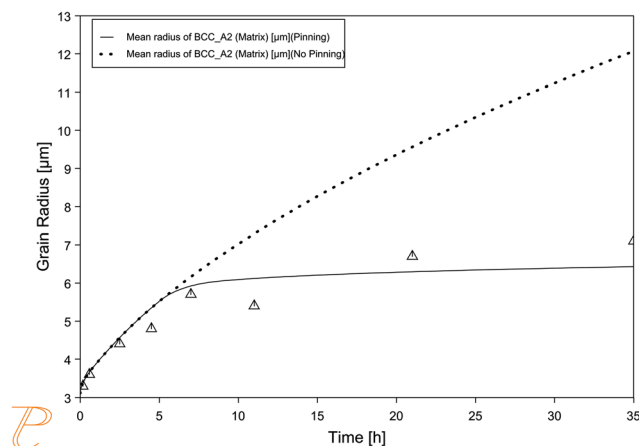

Fig. 8 Calculated average grain size and comparison between un-pinned (dashed line) and pinned (solid line) grain growth. Modified Zener parameters have been used

Interaction of the kinetics between the grains and second phase particles has been revealed as an extremely complicated process, profoundly affected by initial size, grain size distribution, growth and coarsening rate of both phases, to name a few. Inhibition from second phase particles leads to a grain growth significantly deviating from parabolic behavior. In extreme cases, discontinuous grain growth is possible when second phase particles trigger multiple distinctive stopping events. Though this possibility has been qualitatively explained by a numerical experiment, search for further practical evidence is required. For more quantitative analyses, a simplified setup has thus to be utilized in which pre-existing second phase particles are static, refraining from size and volume fraction changes. The non-uniform grain size distribution always gives a limiting average grain size $\overline{R}$ smaller than Zener radius R_z, instead of the equal size assumption from most theoretical and experimental work. Gladman considered the heterogeneity of GSD and derived a dependence of Zener radius on a parameter Z, the ratio of the maximum growing grains to matrix (mean) grains.[22,23] However, practically Z is difficult to be identified precisely, comparing with the more distinct minimum size R_m as shown in Fig. 4. Hellman and Hillert[17] also considered non-uniform GSD, and derived from Eq 16 that, assuming minimum grain size $R_m = 0.75R_{Cr}$ and further $\overline{R} = R_{Cr}$, the limiting average size $\overline{R}$ is one-third of the Zener radius. Qualitatively their conclusion supports our observations. However, they noted that their assumptions were arbitrary, and were not reproduced by the current numerical results to offer a decisive, quantitative guidance. Nevertheless, their assumption can be used as a "lower bound", in that the limiting average grain size is approximately one-third of Zener radius. The current numerical results indicate that for a narrower initial grain size distribution, an "upper bound" of $R_m = 0.5R_{Cr}$ exists, so that R_{Cr}, and approximately the limiting average size $\overline{R}$, is equal to Zener radius, as shown in Fig. 5, corresponding to a uniform grain size distribution approximation assumed in most experimental work. Therefore, K parameter in Zener model, obtained from most literature, e.g. those collected in the overview by Monahar et al.[13] should be multiplied by a factor from 1 (narrower GSD) to 3 (broader GSD) when grain size distribution is taken into account.

Meanwhile, current numerical results cast doubt on the validity of the Zener model during the nucleation and growth stage of second phase precipitation, as experimental data suggested that in this stage it appeared to follow normal grain growth. Admittedly an ill-described precipitation kinetics could have increased the volume fraction of the second phase too quickly. In most cases, however, the volume fraction increase outpaces particle growth

remarkably. Understandably the original derivation of Zener model, and almost all the revisions afterwards, considered a fixed particle size and volume fraction, whose values were naturally chosen from coarsening stage. While the arbitrary "cut-off" size implemented in the current work seems practically effective, an in-depth model development is certainly required. Gottstein and Shvindlerman[24] studied the grain boundary motion in the presence of mobile particles. Their theory suggested that for small second phase particles (high mobility particles), grain boundary motion is controlled by grain boundary mobility (hence un-pinning state), whereas for large particles (low mobility particles) boundary velocity is determined by particle density (hence volume fraction) and particle mobility. This is consistent with current observations. Incorporation of their theory into the current model is in progress. Further improvements are also being investigated, including effect of particle size distribution of second phase,[25] effect of large volume fraction,[16] precipitates at different locations (bulk, grain boundary, grain edges, grain corners, etc.),[17] effect of the precipitate shape,[26–28] etc.

5 Summary

A mean-field model has been developed that enables simulations of normal grain growth in terms of grain size distribution. Integration of this model into a precipitation simulation program, and application of a modified Zener pinning model, also enable the investigation of the interactions between grain growth and precipitation kinetics.

Normal grain growth simulations have been successfully validated against theory to follow a parabolic growth behavior. A steady-state Hillert distribution has been obtained, regardless of the initial grain size distribution.

Second phase particles and their precipitation kinetics dramatically affect the grain growth behavior. A successfully designed validation process also reveals that the average grain size is smaller than Zener radius by up to 3 times when an initially non-uniform grain size distribution is introduced. The practical application of the Zener model awaits further improvements to solve the discrepancy from experimental grain size information at the nucleation and growth stages of precipitation.

References

1. J.E. Morral, and G.R. Purdy, Particle Coarsening in Binary and Multicomponent Alloys, *Scripta Metall. Mater.*, 1994, **30**(7), p 905–908.
2. TC-PRISMA, http://www.thermocalc.com/products-services/software/precipitation-module-(tc-prisma)/
3. K. Wu, J.E. Morral, and Y. Wang, A Phase Field Study of Microstructural Changes Due to the Kirkendall Effect in Two-Phase Diffusion Couples, *Acta Mater.*, 2001, **49**(17), p 3401–3408.
4. M. Hillert, On the Theory of Normal and Abnormal Grain Growth, *Acta Metall.*, 1965, **13**(3), p 227–238.
5. C.S. Smith, Grain Shapes and Other Metallurgical Applications of Topology, in *Metal Interfaces*. C. Herring, Ed., American Society for Metals, Cleveland, 1952, p 65–108
6. J.E. Burke, and D. Turnbull, Recrystallization and Grain Growth, *Prog. Met. Phys.*, 1952, **3**, p 220–292.
7. J.A. Glazier, Grain Growth in Three Dimensions Depends on Grain Topology, *Phys. Rev. Lett.*, 1993, **70**(14), p 2170–2173.
8. J. von Neumann, Discussion-shape of metal grains, metal interfaces, in *American Society of Metals*. C. Herring, Ed., Cleveland, 1952, p 108–110
9. R.D. MacPherson, and D.J. Srolovitz, The Von Neumann Relation Generalized to Coarsening of Three-Dimensional Microstructures, *Nature*, 2007, **446**(7139), p 1053–1055.
10. I.M. Lifshitz, and V.V. Slyozov, The Kinetics of Precipitation from Supersaturated Solid Solutions, *J. Phys. Chem. Solids*, 1961, **15**, p 35.
11. C. Wagner, Theorie Der Alterung Von Niederschlägen Durch Umlösen (Ostwald-Reifung), *Z. Elektrochem.*, 1961, **65**, p 581.
12. C.S. Smith, Grains, Phases, and Interfaces—An Interpretation of Microstructure, *Trans. AIME*, 1948, **175**, p 15–51.
13. P.A. Manohar, M. Ferry, and T. Chandra, Five Decades of the Zener Equation, *ISIJ Int.*, 1998, **38**(9), p 913–924.
14. R. Kampmann, and R. Wagner, *Kinetics of Precipitation in Metastable Binary Alloys -Theory and Application to Cu-1.9 at % Ti and Ni-14 at % Al, Decomposition of Alloys: The Early Stages* Pergamon, London, 1984, p 91–103
15. J. Jeppsson, J. Ågren, and M. Hillert, Modified Mean Field Models of Normal Grain Growth, *Acta Mater.*, 2008, **56**(18), p 5188–5201.
16. M. Hillert, Inhibition of Grain Growth by Second-Phase Particles, *Acta Metall.*, 1988, **36**(12), p 3177–3181.
17. P. Hellman, and M. Hillert, On the Effect of Second-Phase Particles on Grain Growth, *Scandinavian J Metall.*, 1975, **4**, p 211–219.
18. T.R. Malow, and C.C. Koch, Grain Growth in Nanocrystalline Iron Prepared by Mechanical Attrition, *Acta Mater.*, 1997, **45**(5), p 2177–2186.

19. P.A. Beck, J.C. Kremer, L. Demer, and M. Holzworth, Grain Growth in High-Purity Aluminum and in an Aluminum-Magnesium Alloy, *Trans. Am. Inst. Min. Metall. Eng*, 1948, **175**, p 372–400.
20. B.-N. Kim, K. Hiraga, and K. Morita, Kinetics of Normal Grain Growth Depending on the Size Distribution of Small Grains, *J. Jpn. Inst. Metals*, 2004, **68**, p 913–918.
21. P. Feltham, Grain Growth in Metals, *Acta Metall.*, 1957, **5**, p 97–105.
22. T. Gladman, and F. Pickering, Grain-Coarsening of Austenite, *Iron Steel Inst J*, 1967, **205**, p 653–664.
23. T. Gladman, One the Theory of the Effect of Precipitate Particles on Grain Growth in Metals, *Proc. R. Soc. London Series*, 1966, **294**, p 298–309.
24. G. Gottstein, and L.S. Shvindlerman, Theory of Grain Boundary Motion in the Presence of Mobile Particles, *Acta Metall. Mater.*, 1993, **41**(11), p 3267–3275.
25. R.I. Fullman, Boundary migration during grain growth, metal interfaces, in *American Society for Metals*. C. Herring, Ed., Cleveland, 1952, p 179–207
26. N. Ryum, O. Hunderi, and E. Nes, On Grain Boundary Drag from Second Phase Particles, *Scr. Metall.*, 1983, **17**(11), p 1281–1283.
27. E. Nes, N. Ryum, and O. Hunderi, On the Zener Drag, *Acta Metall.*, 1985, **33**(1), p 11–22.
28. S.P. Ringer, W.B. Li, and K.E. Easterling, On the Interaction and Pinning of Grain Boundaries by Cubic Shaped Precipitate Particles, *Acta Metall.*, 1989, **37**(3), p 831–841.

Publisher's Note Springer Nature remains neutral with regard to jurisdictional claims in published maps and institutional affiliations.